Available online at www.sciencedirect.com

ScienceDirect

Geochimica et Cosmochimica Acta 265 (2019) 371–385

Geochimica et Cosmochimica Acta

www.elsevier.com/locate/gca

Vanadium isotopic fractionation during the formation of marine ferromanganese crusts and nodules

Fei Wu [a,b,c], Jeremy D. Owens [a], Limei Tang [d,*], Yanhui Dong [d], Fang Huang [b,*]

[a] Department of Earth, Ocean and Atmospheric Science and National High Magnet Field Laboratory, Florida State University, Tallahassee, FL, USA

[b] CAS Key Laboratory of Crust-Mantle Materials and Environments, School of Earth and Space Sciences, University of Science and Technology of China, Hefei 230026, Anhui, China

[c] Department of Earth and Planetary Sciences, Macquarie University, Sydney, New South Wales 2109, Australia

[d] Key Laboratory of Submarine Geosciences, SOA, Second Institute of Oceanography, MNR, China

Received 27 November 2018; accepted in revised form 3 September 2019; Available online 12 September 2019

Abstract

Vanadium (V) isotopes can be significantly fractionated during the delivery, cycling, and burial to the ocean. The utilization of V isotopes might provide a useful geochemical tracer for the evolution of the oceans. This study provides the first detailed investigation of V isotopes in ferromanganese (Fe-Mn) crusts and nodules, which are widely distributed in the modern oxic ocean. Our results show a large variability of V isotope compositions in Fe-Mn crusts and nodules with a $\delta^{51}V$ range from −0.89 to −1.65‰, much greater than current analytical uncertainty (±0.10‰, 2 SD). Therein, the most recent layers of hydrogenetic Fe-Mn crust and hydrogenous nodules have a narrower V isotope range (−0.89‰ to −1.25‰), with no correlation to their collection location or water depth. Thus, our results suggest a relatively homogeneous V isotope composition of marine hydrogenetic Fe-Mn crusts and nodules, with an average $\delta^{51}V$ of -1.05 ± 0.16‰ (2 SD). The hydrogenetic Fe-Mn crusts and nodules are depleted in ^{51}V compared with the recently reported seawater value (0.2 ± 0.15‰) by $\sim 1.2 \pm 0.2$‰ (2 SD). This can be explained by isotope fractionation during the adsorption of V onto Fe-Mn oxyhydroxides. The various $\delta^{51}V$ in Fe-Mn nodules (−0.98‰ to −1.65‰) might be caused by diagenetic precipitation of V from pore fluids with lighter isotope composition compared to seawater, thus driving a negative V isotope shift recorded in Fe-Mn nodules with a diagenetic imprint. Additionally, a depth profiles across an Fe-Mn crusts reveals systematic changes in $\delta^{51}V$ from -1.04 ± 0.13‰ (2 SD) in upper layers to 1.32 ± 0.06‰ (2 SD) in lower layers representing the relatively older deposition. The observed $\delta^{51}V$ depth profiles might record the changes of V isotope composition of seawater. The proposed temporal variations of $\delta^{51}V$ in seawater could be controlled by the isotope fractionation and fluxes of various V sources and sinks to the ocean that is likely related to the global redox state of the oceans. Another potential interpretation of this isotopic shift in the crusts could be related to the modification of the primary V isotope signature due to diagenetic remobilization and reorganization. However, there is no obvious evidence that definitively documents a diagenetic control or signal. This study highlights the burial of V with Fe-Mn oxyhydroxide as an important control on the V isotope composition of seawater, and the potential application of Fe-Mn crusts to track the temporal V isotope variations of seawater.

Keywords: Paleoceanography; Marine Fe-Mn oxyhydroxides; Mineral adsorption; V mass balance

* Corresponding authors.
E-mail addresses: tanglm@sio.org.cn (L. Tang), fhuang@ustc.edu.cn (F. Huang).

https://doi.org/10.1016/j.gca.2019.09.007
0016-7037/

1. INTRODUCTION

Vanadium is a redox-sensitive element with two geologically long-lived stable isotopes, ^{50}V (~0.25%) and ^{51}V (~99.75%). With recent advances of chemical purification and high-precision measurement using multi-collector inductively-coupled-plasma mass-spectrometry (MC-ICP-MS), the small natural isotopic variations for vanadium can be analytically resolved (Nielsen et al., 2011, 2016; Prytulak et al., 2011; Wu et al., 2016). Recent studies have addressed significant natural V isotope variations in oils, igneous rocks, and meteorites (Gao et al., 2018; Nielsen et al., 2014, 2019; Prytulak et al., 2013, 2017; Schuth et al., 2017; Ventura et al., 2015; Wu et al., 2018, 2019; Xue et al., 2018), documenting that V isotopes can be significantly fractionated in both high- and low-temperature processes.

Vanadium is among the most abundant trace metal elements in seawater, with concentrations between ~30 and 40 nmol/kg (~1.5–2.0 μg per L; e.g. Collier, 1984; Jeandel et al., 1987; Shiller and Boyle, 1987). The residence time of V has been calculated to be between ~ 50 to 100 thousand years (kyrs) in modern seawater (Emerson and Huested, 1991; Morford and Emerson, 1999, Algeo, 2004). Data from the deep ocean suggest that V is uniformly distributed, while surface minima of V have been observed in dozens of vertical surface seawaters profiles in the Pacific Ocean (Collier, 1984; Ho et al., 2018). Additionally, recent work, albeit only from small datasets, suggests that the deep ocean seawater is isotopically homogeneous with $\delta^{51}V_{seawater}$ of $0.20 \pm 0.15‰$ (Wu et al., 2019) and more positive than most silicate rocks (−0.9 to −0.5‰, Prytulak et al., 2013; Wu et al., 2016, 2018; Qi et al., 2019), and river water (Schuth et al., 2019).

The speciation and behavior of V are controlled by the Eh, pH, and V concentrations in seawater. The main species of V in oxic seawater are highly soluble pentavalent vanadate (e.g. HVO_4^{2-} and $H_2VO_4^-$; Lewan and Maynard, 1982). Vanadate tends to be adsorbed on the surface of iron (Fe) and manganese (Mn) oxyhydroxides or clay minerals, which is a dominate sink of V in modern seawater (Elderfield and Schultz, 1996, Morford and Emerson, 1999). Under mildly reducing conditions, pentavalent vanadate tends to be reduced to tetravalent vanadyl (e.g. VO^{2+}, $VO(OH)_3^+$) by organic compounds. Vanadyl is less soluble than vanadate and readily adsorbed onto settling particles (Breit and Wanty, 1991). Under strongly reducing conditions, vanadyl can be further reduced to trivalent species (e.g. $V(OH)_3$) through reactions with sulfide in the water column or pore water (Wanty and Goldhaber, 1992). Trivalent V is highly insoluble in seawater and tends to precipitate as solid oxyhydroxides (Wehrli and Stumm, 1989). Theoretical calculation predicts that V isotopes can be fractionated during the uptake and accumulation of V in marine sediments (Wu et al., 2015), which is likely controlled by variations in the redox state and surface adsorption (e.g., Algeo and Maynard, 2004; Huang et al., 2015; Morford and Emerson, 1999). Recent studies of V isotope compositions of crude oils have revealed large V isotope fractionation up to ~2‰, likely reflecting the depositional redox conditions of the petroleum source rock and the post-burial modification such as maturation and/or biodegradation (Ventura et al., 2015; Gao et al., 2018). In addition, the redox potential of V(V)-V(IV) couple is close to that of Fe (III)-Fe(II) in seawater (e.g. Bonatti et al., 1971; Piper and Calvert, 2009), which suggests that V sequestration from the water column under reducing conditions does not require free hydrogen sulfide (Breit and Wanty, 1991; Morford and Emerson, 1999; Algeo and Maynard, 2004). Thus, V isotope systematics can be used to trace ocean redox variations, especially the variations of anoxic but non-sulfidic seafloor area at local and/or global scales. Despite the potential application of V isotopes as a paleo-redox proxy, the lack of $\delta^{51}V$ data in marine materials restricts the understanding of the controlling mechanisms of V isotope fractionation in marine sediments.

Ferromanganese oxyhydroxide deposit is globally distributed throughout the marine seafloor (e.g. Hein and Koschinsky, 2014, and references therein) and is an important oceanic sink for many trace metals (e.g. Koschinsky and Hein, 2003; Barling and Anbar, 2004; Rehkämper and Nielsen, 2004). In addition, scavenging of V to oxic sediment by the adsorption of V onto hydrogenetic Fe–Mn oxyhydroxides is one of the dominate mechanisms for removing V from the well-oxygenated modern ocean (Morford and Emerson, 1999). Thus, to build a mass balance framework for V isotopes, it is important to constrain the natural isotope fractionation of V during incorporation into Fe–Mn oxyhydroxides. The $\delta^{51}V$ values of two marine Fe-Mn nodules NOD-P ($-1.65 \pm 0.06‰$) and NOD-A ($-0.99 \pm 0.10‰$) have previously been reported (Wu et al., 2016), suggesting that large V isotope fractionation could occur during the formation of Fe-Mn oxyhydroxides. Comparing this result with the recently reported V isotope composition of seawater ($0.20 \pm 0.15‰$; Wu et al., 2019) implies that Fe-Mn deposits are significantly depleted in ^{51}V relative to seawater. Theoretical calculations show that the light V isotope (^{50}V) is preferentially adsorbed on the surface of Fe oxyhydroxides (Wu et al., 2015), which could explain the V isotope offset between natural Fe-Mn deposits and seawater. But the limited data of $\delta^{51}V$ for natural Fe-Mn deposits do not allow for further testing of this hypothesis. In addition, a preliminary estimation of the V isotope mass balance for the oceans was made based on the seawater V isotope data and marine Fe-Mn nodules, implying that burial of V with Fe–Mn oxyhydroxides precipitation could be an important isotopically light sink in the modern ocean (Wu et al., 2019).

Marine Fe–Mn precipitates throughout the oceans are generally classified as hydrogenetic, diagenetic, or hydrothermal deposits (e.g. Hein et al., 1997; Bau et al., 2014). Such classification reflects their discrete formation environment and respective modes of accretion. Moreover, they exhibit distinct differences both in terms of appearance, mineralogy, growth rates and trace element composition (e.g., Glasby, 2006). Therein, hydrogenetic Fe-Mn precipitates could form as crusts and nodule aggregations (e.g. Glasby, 2006), or as micro-nodules and ferromanganese coatings on other sediment grains in the pelagic sediments (e.g., Dunlea et al., 2015). Their formation is

attributed to the direct precipitation and aggregation of colloidal material from ambient seawater (Dymond et al., 1984). In comparison, diagenetic Fe-Mn precipitates are typically formed as nodules and grow at the sediment-water interface of pelagic sediments (Dymond et al., 1984). The growth and trace-metal composition of diagenetic nodules are largely controlled by early diagenetic processes within the sediments with the contribution of metals from the sediment porewaters (e.g. Calvert and Price, 1977; Dymond et al., 1984; Jung and Lee, 1999). Considering that Fe-Mn nodules could form by hydrogenetic or diagenetic precipitation, or a combination (Hein et al., 1997), systematic studies of V isotopic compositions of Fe-Mn deposits are necessary for better understanding V isotope fractionation in the Fe-Mn nodules associated with sequestration of V from seawater and/or pore fluids (Wu et al., 2016).

In this study, we present spatiotemporal variations of $\delta^{51}V$ in Fe-Mn crusts, and investigate the controlling factors of V isotope variations in Fe-Mn nodules. Hydrogenetic Fe-Mn crusts mainly consist of Fe-Mn oxyhydroxides that precipitate directly from ambient seawater. Thus, the V isotope investigation of modern Fe-Mn crusts is helpful for understanding the V isotope fractionation during the adsorption of V on the Fe–Mn oxyhydroxides. In addition, because of the slow growth rates of hydrogenetic Fe-Mn crusts (1–10 mm/Myr; Hein et al., 2000; Glasby, 2006), they have been applied as archives of past chemical and isotopic compositions for many elements to better constrain deep seawater records (e.g. Nd, Fe, Ni, Tl) (Ling et al., 1997; Frank et al., 1999; Nielsen et al., 2009; Gall et al., 2013; Horner et al., 2015; Gueguen et al., 2016). Thus, we also investigated the depth profiles of V isotopes in one Fe-Mn crust. The major and trace element concentrations of these marine Fe-Mn crusts and nodules were also analyzed to constrain their genetic types. The goals of this study are to investigate: (1) isotope fractionation due to the removal of V via adsorption onto Fe-Mn crusts from seawater, (2) the mechanism for V isotope variations in Fe-Mn nodules, and (3) the potential utility of Fe-Mn crusts as archives for deep seawater V isotope compositions and its implications on the reconstruction of paleo-environmental changes.

2. SAMPLE SELECTION AND PREPARATION

The Fe-Mn crusts and nodules studied here were collected at 2013 from three seamounts or guyots at the West Pacific Ocean using the Chinese manned submersible Jiaolong during DY125-31 cruise. Samples were from Caiwei Guyot (155° E, 15° N) and Caiqi Guyot (154° E, 15° N) from the Magellan Seamount cluster, and Weiyuan Seamount (154° W, 9° N) from Clarion-Clipperton Fe-Mn Nodule Zone (C-C zone) (Fig. 1, Table 1) at water depths of 1720–4420 m, 2000–2400 m and 5200 m, respectively. The samples studied here were obtained from the surface of the seafloor to avoid the potential diagenetic process that have occurred post burial (e.g. Heller et al., 2018). All samples from Caiwei Guyot and Caiqi Guyot are Fe-Mn crusts, while samples from Weiyuan Seamount include both Fe-Mn crusts and nodules. Some samples are from the surface layer of the ferromanganese crust to study the spatial variations of V isotope of 'recently' or near modern precipitated ferromanganese crust (Table 2). Furthermore, some Fe-Mn crust samples (Table 2) were sawed perpendicular to growth layers, which best represents a stratigraphic record of ocean chemistry.

Vanadium isotopic compositions of two USGS international standards NOD-P-1 and NOD-A-1 were previously reported in (Wu et al., 2016). NOD-P-1 was collected from the Pacific Ocean (14°50′ N, 124°28′ W, Clarion-Clipperton Fe-Mn Nodule Zone) at a depth of 4,300 meters, and NOD-A-1 was collected from the Atlantic Ocean along the Blake Plateau (31° 02′ N, 78° 22′ W) at a depth of 788 meters (Flanagan and Gottfried, 1980). The data of these two Fe-Mn nodule standards are discussed with other samples in this work.

3. ANALYTICAL METHODS

3.1. Whole-rock major and trace elements

The collected Fe-Mn crust and nodule samples were first cleaned by ultrasonication with deionized water and then dried in an oven at 105 °C for six hours. Then samples were powdered using an agate mortar and pestle until the sample passed through a 200 mesh sieve. Prior to powdering, crust samples were cut into layers using a hacksaw with a vertical thickness of 1–3 cm. Nodule samples with diameters of 2–5 cm were cut in half from center prior to powdering. Whole-rock major and trace element measurements of Fe-Mn crusts and nodules were conducted at the ALS Laboratory Group in Guangzhou, China (http://www.alsglobal.net.cn/). The sample powders were combined with lithium borate flux and fused in a furnace at ~1000 °C. The resulting melt was then cooled and dissolved in nitric acid and hydrochloric acid. This solution was then analyzed by Inductively Coupled Plasma Atomic Emission Spectroscopy (ICP-AES) for major elements measurements. For trace element measurements, the powders were digested with a mixture of perchloric, nitric and hydrofluoric acids, and then dissolved with dilute hydrochloric acid. The prepared solutions were then analyzed by Inductively Coupled Plasma Mass Spectrometry (ICP-MS). Several standard reference materials were analyzed to access accuracy, precision and reproducibility for major (GBW07107 and GBW07108) and trace (GBM908-10, GBM908-5, MRGeo08, OREAS 90) elements measurements, respectively. The results are shown in Table S1. Analytical accuracy and precision are better than ±2% for major elements and better than ±5% for the elements discussed here. The major and trace element compositions of Fe-Mn crusts and nodules are listed in Table 2.

3.2. Vanadium isotope analyses

Approximately 10–20 mg of sample powders containing 5–10 μg of V were digested for V isotope analysis. Samples were first treated with aqua regia. After evaporation to dryness, samples were dissolved with a 3:1 (v/v) mixture of concentrated HF and HNO_3 to digest the remaining oxide

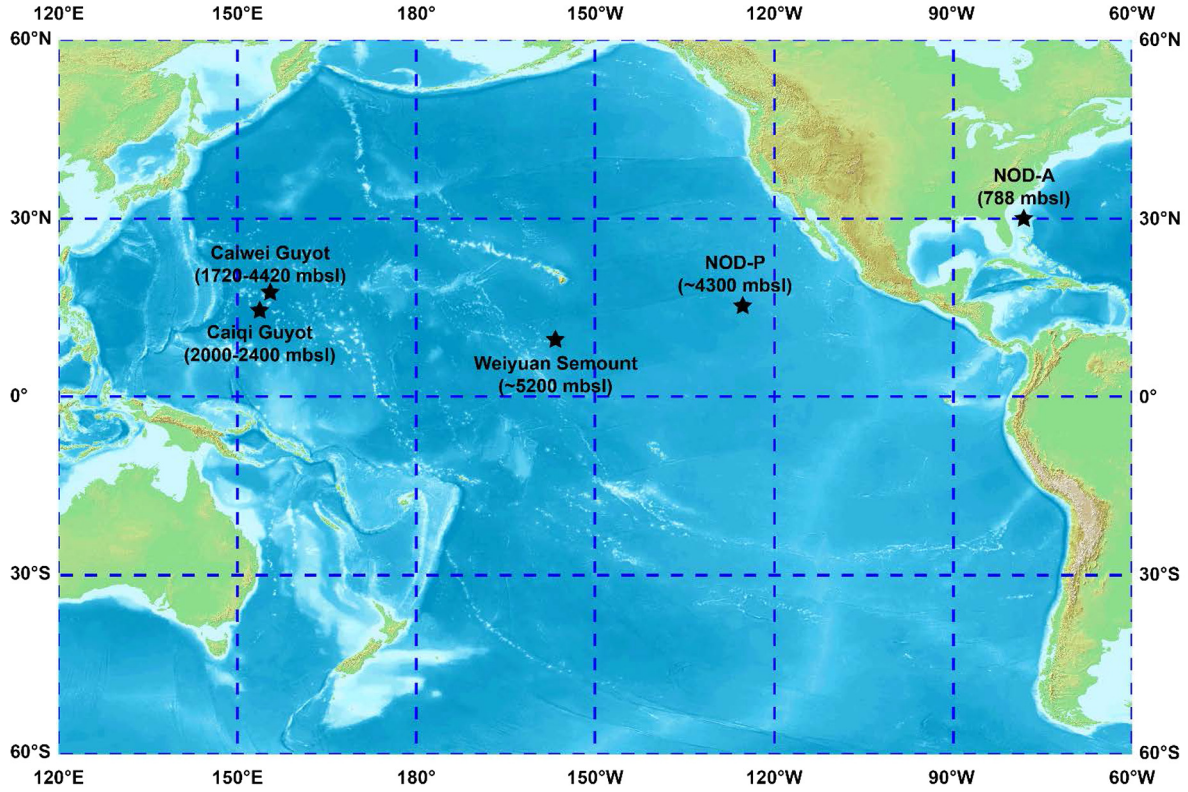

Fig. 1. Map showing the locations of Fe-Mn crusts and nodules samples. Black stars show sample locations. Also shown is the range of depositional depths in meters below sea-level (mbsl) for the samples. More details of sample location and description are in Table 1.

Table 1
Location of the ferromanganese crusts and nodules samples.

Sample No.	Cruise No.	Type	Water depth (mbsl)	Longitude	Latitude
Weiyuan seamount					
Dive64A OR512-121T	Dive 64	Crust	5200	154°17.8′ W	9°59.8′ N
Dive64A OR512-141T	Dive 64	Nodule	5200	154°17.8′ W	9°59.8′ N
Dive64A OH200-111T(2)	Dive 64	Nodule	5200	154°17.8′ W	9°59.8′ N
Dive64A OH200-111T(3)	Dive 64	Nodule	5200	154°17.8′ W	9°59.8′ N
Dive68 OH200-011T(1)	Dive 68	Nodule	5100	153°3.7′ W	6°44.6′ N
Dive68 OH200-011T(2)	Dive 68	Nodule	5100	153°3.7′ W	6°44.6′ N
Caiwei Guyot					
Dive69 OJ121-111T	Dive 69	Crust	4420	155°24.0′ E	15°25.8′ N
Dive70A OJ112-112T	Dive 70	Crust	1954–2230	155°33.0′ E	15°55.2′ N
Dive70A OJ121-121T	Dive 70	Crust	1954–2230	155°33.0′ E	15°55.2′ N
Dive70B OJ113-211T	Dive 70	Crust	2350–2500	155°33.0′ E	15°55.2′ N
Dive70C OJ111-314T	Dive 70	Crust	2350–2500	155°33.0′ E	15°55.2′ N
Dive71 OJ112-011T	Dive 71	Crust	1720	155°25.2′ E	15°52.8′ N
Caiqi Guyot					
Dive73 OJ110-012T	Dive 73	Crust	2000–2400	154°58.2′ E	15°9.0′ N
Dive73 OJ110-021T	Dive 73	Crust	2000–2400	154°58.2′ E	15°9.0′ N
Dive73 OJ110-033T	Dive 73	Crust	2000–2400	154°58.2′ E	15°9.0′ N
Dive73 OJ120-011T	Dive 73	Crust	2000–2400	154°58.2′ E	15°9.0′ N
Dive73 OJ120-021T	Dive 73	Crust	2000–2400	154°58.2′ E	15°9.0′ N
Nod-P		Nodule	4300	124°28′ W	14°50′ N
Nod-A		Nodule	788	78°22′ W	31°2′ N

and silicate phases. Then, samples were dried and further treated with aqua regia and concentrated HNO_3 and dried down in between each step. All the samples were finally dissolved in 1 mL of 1 M HNO_3 for ion-exchange chromatography.

The details of the V chemical purification protocol and isotopic measurement procedure are described in great details in Wu et al. (2016). Briefly, V was purified with a multistep ion-exchange procedure by coupling cation- and anion-exchange columns. The cation resin AG50W-X12

Table 2
Concentrations of selected elements and V isotopic compositions for the ferromanganese crusts and nodules samples.

	Type	Section (cm)	$\delta^{51}V$	2 SD[a]	n[b]	Si wt.%	Al wt.%	Mn wt.%	Fe wt.%	P wt.%	Li ppm	V ppm	Co ppm	Ni ppm	Cu ppm	Zn ppm	Mn/Fe
Weiyuan Seamount																	
Dive64A OR512-121T	Crust	Bulk	−1.04	0.08	7	5.74	1.65	19.5	20.3	0.29	11	719	1530	2520	2230	532	0.96
Dive64A OR512-141T	Nodule	Bulk	−1.40	0.01	3	8.38	2.86	24.6	8.3	0.24	118	456	2220	9863	5810	838	2.96
Dive64A OH200-111 T(2)	Nodule	Bulk	−1.31	0.03	3	7.98	3.16	23.2	10.6	0.20	63	483	2250	8000	5140	704	2.19
Dive64A OH200-111 T(3)	Nodule	Bulk	−1.33	0.08	3	6.51	2.64	25.7	9.5	0.21	82	517	2440	10,442	6980	822	2.71
Dive68 OH200-011 T(1)	Nodule	Bulk	−1.59	0.05	7	6.18	2.46	29.8	6.1	0.17	130	406	1535	12,764	13,595	1330	4.92
Dive68 OH200-011 T(2)	Nodule	Bulk	−1.63	0.10	4	6.23	2.58	30.2	5.0	0.17	119	406	1330	13,194	15,078	1270	6.00
Replicate			−1.64	0.04	3												
Caiwei Guyot																	
Dive69 OJ121-111T	Crust	0–1	−0.89	0.08	3	6.58	1.64	17.0	19.5	0.36	4	493	3440	1750	1025	395	0.87
Dive70A OJ112-112T	Crust	Bulk	−1.17	0.02	3	3.36	0.88	24.3	15.4	0.65	8	546	4840	5380	1295	637	1.58
		0–1	−1.25	0.06	3	4.85	0.91	23.0	16.3	0.36	3	511	5600	3690	632	464	1.41
		1–3.5	−1.10	0.06	5	3.38	1.07	25.4	14.1	0.33	9	530	4520	5960	1600	686	1.81
	Crust	3.5–5.5	−1.28	0.06	3	1.40	0.37	22.8	11.0	2.82	2	506	3500	4450	1405	566	2.08
Dive70A OJ121-121T	Crust	0–1	−1.02	0.06	3	4.51	0.98	23.8	16.3	0.38	4	608	5120	4670	982	552	1.46
		1–4	−1.09	0.01	3	3.92	1.21	23.6	16.0	0.35	6	522	4220	4870	1605	664	1.47
Dive70B OJ113-211T	Crust	1–2	−1.02	0.03	3	3.59	0.62	24.6	17.1	0.36	1	751	5430	3530	847	487	1.44
		2–3	−0.97	0.02	3	4.00	0.81	23.8	17.7	0.34	1	586	5010	3340	1300	534	1.35
		3–4	−1.08	0.09	3	2.89	0.72	25.9	15.8	0.36	2	641	5380	4750	1975	605	1.65
		4–5	−1.14	0.07	6	2.86	0.93	21.7	10.9	3.08	3	431	3510	5630	1835	579	1.99
		5–6	−0.98	0.07	6	2.70	0.88	12.4	9.4	6.42	4	366	1685	2520	1200	386	1.32
		6–7	−1.07	0.07	3	2.08	0.61	17.2	12.5	4.58	2	591	2430	2420	1490	493	1.37
		7–8	−1.30	0.07	3	1.51	0.37	21.9	12.5	3.51	1	707	2460	2600	1360	490	1.76
		8–9	−1.36	0.09	6	1.34	0.32	22.4	11.0	3.83	1	678	3060	2960	1160	496	2.03
		9–10	−1.31	0.07	6	1.61	0.33	22.7	11.3	3.42	1	706	3410	3130	967	480	2.01
Dive70C OJ111-314T	Crust	Bulk	−1.01	0.08	7	4.12	0.88	22.8	16.1	0.34	3	572	5370	3810	997	511	1.42
		0–3.5	−1.05	0.07	5	3.74	0.96	23.4	15.1	0.32	4	575	4830	4500	1610	605	1.54
		3.5–6	−1.00	0.04	7	4.07	0.78	22.5	16.0	0.34	2	625	5260	3620	898	487	1.41
Dive71 OJ112-011T	Crust	Bulk	−0.91	0.07	3	5.62	1.62	21.0	16.0	0.34	6	493	5410	3770	928	475	1.31
Caiqi Guyot																	
Dive73 OJ110-012T	Crust	Bulk	−1.08	0.05	3	5.12	0.95	22.1	18.8	0.45	2	631	5640	3320	792	465	1.18
		0–2	−1.10	0.02	3	2.32	0.39	27.5	15.3	0.34	1	666	7240	5010	852	542	1.80
Dive73 OJ110-021T	Crust	Bulk	−1.05	0.05	3	3.44	0.71	24.4	17.5	0.36	3	721	5420	4210	1195	568	1.39
Dive73 OJ110-033T	Crust	Bulk	−1.09	0.04	3	2.83	0.56	26.2	16.1	0.38	2	598	6500	4720	979	522	1.62
		0–2	−1.15	0.09	3	2.12	0.32	28.0	14.8	0.35	1	611	7110	4860	657	500	1.89
		2–5	−1.04	0.02	3	3.50	0.91	24.2	15.1	0.34	5	591	5350	4670	1295	533	1.61
Dive73 OJ120-011T	Crust	Bulk	−1.10	0.07	3	3.07	0.73	22.7	14.5	1.75	4	662	4220	4350	1390	595	1.56
Dive73 OJ120-021T	Crust	Bulk	−1.12	0.04	6	3.10	0.75	23.3	15.0	1.48	3	588	4610	4270	1085	563	1.56
		0–2.5	−0.99	0.03	3	4.23	0.97	23.8	16.5	0.35	3	616	5670	4140	998	514	1.44
Nod-P	Nodule	Bulk	−1.57	0.09	4	6.49	2.54	29.1	5.8	0.20	140	570	2240	13,400	11,500	1600	5.01
Reference			−1.65	0.06	10												

Nod-A	Nodule	Bulk														
Reference		−0.98	0.01	3	1.78	2.05	18.5	10.9	0.61	76	770	3110	6360	1100	590	1.70
		−0.99	0.10	19												
Pacific pelagic clay					25.6	8.79	0.43	5.39	0.11		117	113	210	230	165	
Upper continental crust					31.1	8.15	0.08	3.92	0.07	21	97	17	47	28	67	

[a] 2 SD is 2 times the standard deviation of the population of n repeat measurements.
[b] n is the number of repeated measurements of the same solution.
[c] Replicate represents repeated dissolution and analysis.
[d] The literature results are from Wu et al. (2016).
[d] Pacific Pelagic Clay data are from Bischoff et al. (1979).
[d] Average upper continental crust. Data are from Rudnick and Gao (2003).

(200–400 mesh) was applied to remove Fe, Ti, and other main matrix elements (e.g., Al, Ca, Mn, and Cr). Then AG1-X8 (200–400 mesh) chloride-form anion resin was used to further remove residual matrix and isobaric elements (e.g., K, Na, Mg, and trace amount of Cr). The total procedural blank is less than 2 ng, thus is negligible compared with the loaded amount of V (5–10 μg). The V yields of the total chemical procedures are >99%. Vanadium isotopic ratios were measured using a sample-standard bracketing method on a Thermo Scientific Neptune plus Multi-Collector Inductively Coupled Plasma-Mass Spectrometer (MC-ICP-MS) at the University of Science and Technology of China (USTC) using an Aridus II desolvating nebulizer (CETAC Technologies) for sample introduction. Measurements were performed at medium-resolution mode (resolution $\Delta M/M > 4000$) to discern the isotope of target elements from isobaric interfering molecular species such as $^{36}Ar^{14}N^+$, $^{36}Ar^{16}O^+$, and $^{38}Ar^{14}N^+$ (Nielsen et al., 2016; Wu et al., 2016). A 10^{10} Ω amplifier was used to monitor the signal of ^{51}V. The typical sensitivity of ^{51}V was ~150 V/ppm. All sample and standard solutions were introduced into the instrument with a V concentration of 0.8 ppm to reduce matrix effects, producing enough signal intensity of ^{50}V (~300 mV) for high-precision analyses. Although our chemical procedure should ensure quantitative removal of Cr and Ti, we simultaneously measured ^{49}Ti and ^{53}Cr to accurately correct any potential interferences of ^{50}Ti and ^{50}Cr on ^{50}V. Sample-standard bracketing method was applied to calibrate instrument mass discrimination effects, using the aliquots of the Alfa Aesar (AA) V standard solution made and distributed by Nielsen et al. (2011) and Prytulak et al. (2011) as the bracketing solution. Vanadium isotopic data are reported in a δ notation of per mil compared to this AA V standard ($\delta^{51}V = (((^{51}V/^{50}V)_{sample}/(^{51}V/^{50}V)_{AA} - 1) \times 1000$ (‰)).

The data quality of V isotope analyses was monitored using a variety of in-house standards, international reference materials, and duplicated samples. The $\delta^{51}V$ values of the nodule standards are -1.57 ± 0.09‰ (2 SD, n = 4, NOD-P) and -0.98 ± 0.01‰ (2 SD, n = 3, NOD-A), within analytical error of previously reported values (Table 2) (NOD-P: -1.65 ± 0.06‰, n = 10 and NOD-A: -0.99 ± 0.10‰, n = 19, Wu et al., 2016). The reproducibility of in-house standards and duplicated samples for V isotope analyses are always better than 0.10‰ (2 SD).

4. RESULTS

The Fe-Mn crust and nodule samples show enrichment of Mn, Fe and trace transition metal (such as V, Co, Ni, Cu, and Zn) compared to Pacific Ocean pelagic clays and average upper continental crust (Bishoff et al., 1979; Rudnick and Gao, 2003) (Table 2). Therein, the nodule samples from Weiyuan Seamount have Mn/Fe ratios from 2 to 6, Cu + Ni contents from ~1 wt.% to 2.8 wt.%, these values are much higher than that of crust samples from Weiyuan Seamount and Caiwei and Caiqi Guyot, which have Mn/Fe ratios lower than 2 and Cu + Ni contents lower than 0.7 wt.% (Table 2). The nodule samples from Weiyuan Seamount also have lower V contents (400–

500 ppm) compared with the crust samples collected at a nearby locality (719 ppm) (Table 2). All the crusts and nodules samples in this work have V/Al ratios of 15.3–211.7 ($\times 10^{-3}$), higher than at least an order of magnitude than that of average Pacific Pelagic Clay (1.3×10^{-3} Bischoff et al., 1979) and upper continental crust (1.2×10^{-3} Rudnick and Gao, 2003) (Table 2). Some Fe-Mn crust samples collected from Caiwei Guyot and Caiqi Guyot show evidence for phosphatization with high concentrations of P (1.48–6.42 wt.%) and Ca (5.47–18.6 wt.%) relative to other samples (Ca < 3 wt.% and P < 1 wt.%) (Table 2).

The $\delta^{51}V$ of the studied Fe-Mn crusts and nodules range from −0.89‰ to −1.63‰ (Table 2), much lower than the seawater values (0.20 ± 0.15‰, Wu et al., 2019). For the samples from Weiyuan Seamount, where both Fe-Mn crusts and nodules were collected, the $\delta^{51}V$ of nodule samples (−1.33‰ to −1.63‰) are significantly lower than that of the crust sample (−1.04‰) (Table 1).

5. DISCUSSION

5.1. Geochemistry and genesis of the Fe-Mn crusts and nodules

Marine Fe–Mn crusts and nodules are distinguished by their morphology and form by different genesis. Fe-Mn crusts are mainly of hydrogenetic genesis that precipitate directly from ambient cold seawater (e.g. Hein et al., 1997), with growth rate less than ~10 mm/Ma (Glasby, 2006). The formation of Fe-Mn crusts can be influenced by the hydrothermal fluids near hot-spot volcanoes, active volcanic arcs, and spreading centers (Hein et al., 1997). In contrast, Fe-Mn nodule formation can be characterized as either hydrogenetic or diagenetic genesis, or by a combination of both processes (Hein et al., 1997). Diagenetic precipitation occurs near the sediment-seawater interface, under the influence of sub-oxic pore fluids from the sediment column underneath (Hein and Koschinsky, 2014), with growth rate of ~10–100 mm/Ma (Glasby, 2006). The difference in deposition modes for Fe-Mn can result in various sources of major and minor metals (Bau et al., 2014). Marine Fe-Mn crusts and nodules also display diverse morphological, mineralogical, and chemical properties (Halbach et al., 1981). Under diagenetic conditions, 10 Å manganates (buserite and todorokite) formed as the main Mn-oxyhydroxide phase (Atkins et al., 2014). Because of the large tunnel-structure of todorokite, cations like Ni, Cu, and Zn that are mobilized from the sediment during oxic diagenesis tend to be incorporated into its crystal structures (Glasby, 2006). Diagenetic and transitional Fe-Mn nodules can also incorporate significant amounts of Li from seawater into the 10 Å manganates (buserite and todorokite, Jiang et al., 2007). In addition, diagenetic Fe-Mn nodules generally have higher Mn/Fe ratios relative to the hydrogenous crusts and nodules (Hein et al., 1997). This is because manganese and iron reduction processes do not occur simultaneously in the diagenetic sequence, and the environmental conditions that are typical for diagenetic Fe-Mn nodule growth occur in zones where upward migration of reduced Mn^{2+} in the pore water start to become re-oxidized (Kuhn et al., 2017). This causes Mn-Fe elemental fractionation within diagenetic layers of manganese nodules with higher Mn/Fe ratio (Wegorzewski and Kuhn, 2014). Considering that marine Fe-Mn crusts and nodules could form by several processes, we will first discern the genesis of these Fe-Mn crust and nodule samples based on their geochemical features.

All the Fe-Mn crust samples in this study are located in Bonatti's field of hydrogenetic growth on the ternary diagram of (Ni + Cu + Co) × 10-Fe-Mn (Fig. 2), showing that they are hydrogenetic in origin without influence of hydrothermal overprinting (Bonatti, 1972; Menendez et al., 2019). The thick Fe-Mn crusts show a dual structure with distinct geochemical features between the upper portion (younger non-phosphatized layers) and the underlying lower portion (older phosphatized layers). Therein, the older phosphatized layers of the Fe-Mn crusts have been impregnated with carbonate fluorapatite (CFA) with enrichments of phosphorus (Table 2) during episodes of phosphatization in the late Eocene through middle Miocene (Hein et al., 1993, 2000).

The studied Fe-Mn nodule samples are located in Bonatti's field of hydrogenetic, diagenesis, and mixed growth (Fig. 2). Therein, the Mn/Fe ratios of Fe-Mn crust and nodules from Weiyuan seamount (C-C zone) are also positively correlated with Cu + Ni (also Zn) and Li concentrations (Fig. 3). The Weiyuan crust sample shows the lowest Mn/Fe, Li and Cu + Ni concentrations among all samples from Weiyuan seamount and is within the range of other crust samples from West Pacific (Fig. 3). Taking this crust sample as the hydrogenous endmember of Weiyuan Fe-Mn crusts and nodules, the correlation trend between the Mn/Fe and the metals shown in Fig. 3 may indicate that various extents of diagenesis could influence the chemical compositions of Fe-Mn nodules. The reference material NOD-P, which was also collected from the C-C

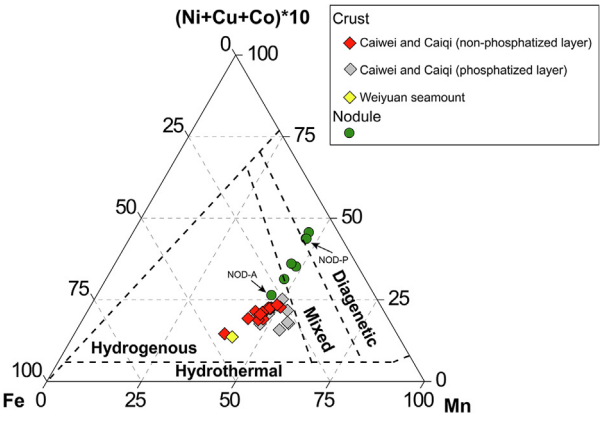

Fig. 2. Ternary diagram with Mn, Fe, and (Co + Ni + Cu) × 10 for all Fe-Mn crusts and nodules of this study. Dashed black lines define different fields, corresponds to hydrogenetic growth, diagenetic growth, mixed growth, and hydrothermal growth conditions (with fields modified from Bonatti, 1972 and Menendez et al., 2019). All the crust samples in this study are in the hydrogenetic area of the ternary diagram while the nodule samples distribute in hydrogenetic, diagenetic and mixed areas.

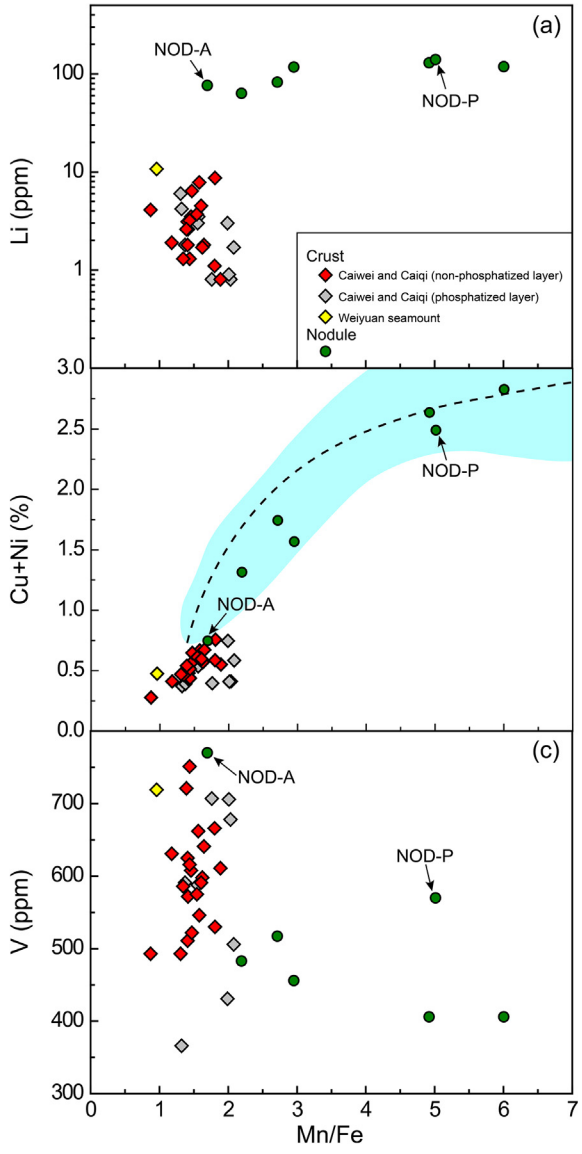

Fig. 3. Mn/Fe ratios versus Li (a), Cu + Ni (b), and V (c) in Fe-Mn crusts and nodules samples. All the nodule samples except NOD-A in this study are from C-C zone. The area and dotted line in (b) also show the variation and hyperbolic regression curve of Ni + Cu against Mn/Fe for the diagenesis nodules from the C-C zone (after Halbach et al., 1981). The crusts and nodules show obviously chemical distinctions.

zone, also fits this trend between Mn/Fe and trace metals (Fig. 3). In contrast, the geochemical features of NOD-A (Mn/Fe ratio, Cu, Ni, and Zn contents) are similar to the hydrogenous Fe-Mn crust although it shows an enrichment in Li. The NOD-A nodule is also located in Bonatti's field of hydrogenetic growth on the ternary diagram of (Ni + Cu + Co) × 10-Fe-Mn (Fig. 2). Thus, we conclude that the studied Fe-Mn nodules from the C-C zone (Weiyuan seamount and NOD-P) are mainly influenced by diagenesis and should be considered as diagenetic nodules, while NOD-A is more likely from a hydrogenetic nodule that is not significantly affected by diagenetic imprint.

In the discussion below, we will first discuss the fractionation of V isotope between hydrogenic Fe-Mn crusts/nodules and seawater with the results of non-phosphatized crust samples and hydrogenic nodule sample NOD-A. Then, we will discuss if/how diagenetic formation influences the V isotope composition of marine Fe-Mn nodules with the results of diagenesis nodule samples. Lastly, we will investigate the possibility to apply Fe-Mn crusts as archives to record paleo-ocean V isotope variations, by discussing the controlling of the V isotope variations for the depth profile of Fe-Mn crusts.

5.2. The control of V isotope fractionation in the hydrogenic Fe-Mn crusts and nodules

Due to the slow growth rate of hydrogenous Fe-Mn crusts, the accumulation history could be over many millions of years thus the measured isotope values are an integration of several million years. Although the age data for these samples are not exactly known, the non-phosphatized upper layers of these Fe-Mn crust samples from equatorial Pacific were thought to have formed during the Miocene likely younger than 10–17 million years old (Hein et al., 1993; Hyeong et al., 2013; Nishi et al., 2017). The non-phosphatized layers of these Fe-Mn crust samples are characterized by limited V isotope variations, with $\delta^{51}V$ values between −0.89‰ and −1.25‰ (Table 2 and Fig. 4). The Mn/Fe ratios and V concentrations of these Fe-Mn crust samples do not document clear correlations with $\delta^{51}V$ ($R^2 = 0.34$ for Mn/Fe vs $\delta^{51}V$ and $R^2 = 0.00$ for V vs $\delta^{51}V$, Fig. 4). The hydrogenous Fe-Mn nodule, NOD-A, also has a $\delta^{51}V$ value (−0.99‰) similar to the Fe-Mn crust samples (−0.89‰ to −1.25‰). In addition, there is no clear $\delta^{51}V$ difference for samples collected at various water depths below 500 m (Fig. 5) or from different ocean seamounts. The limited variation of $\delta^{51}V$ in these hydrogenous Fe-Mn crusts and nodules regardless of their elemental geochemistry, location and depositional water-depth implies that $\delta^{51}V$ in younger non-phosphatized hydrogenetic ferromanganese crusts and nodules are uniform throughout the oceans, with an average of -1.05 ± 0.16‰ (2 SD, n = 22).

Hydrogenetic Fe-Mn crusts and nodules grow by incorporation of Fe- and Mn-oxyhydroxide precipitates from seawater and scavenge dissolved trace elements from the water column. Considering the long residence time of V (50–100 kyrs) relative to the circulation time of the ocean (~2 kyrs) and the homogeneous V concentrations of deep seawater (Collier, 1984; Ho et al., 2018; Jeandel et al., 1987; Shiller and Boyle, 1987), it is highly likely that V in the deep ocean is well mixed. It is also suggested that V isotopic composition of open ocean seawater is homogeneous across major ocean basins albeit with limited data, with $\delta^{51}V$ of 0.20 ± 0.15‰ (Wu et al., 2019). Thus, $\delta^{51}V$ in near modern Fe-Mn crusts and nodules are systematically fractionated by -1.2 ± 0.2‰ (2 SD) from the starting seawater values.

A possible mechanism for the V isotopic offset between seawater and hydrogenous Fe-Mn crusts and nodules is the isotope fractionation during the adsorption of V on the surface of the Fe-Mn oxyhydroxide. Theoretical calculation

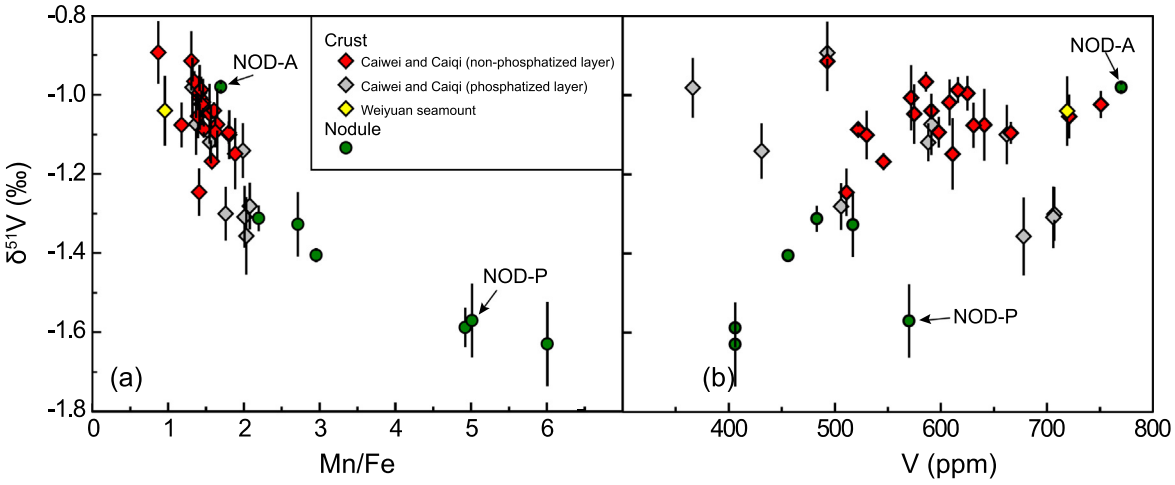

Fig. 4. Mn/Fe ratios (a) and V (b) versus $\delta^{51}V$ in Fe-Mn crusts and nodules samples. The Mn/Fe ratio and V concentrations of Fe-Mn crust samples show no clear correlation with $\delta^{51}V$ ($R^2 = 0.34$), while the $\delta^{51}V$ of the deep-water diagenetic nodules display a negative correlation with Mn/Fe ratio ($R^2 = 0.85$).

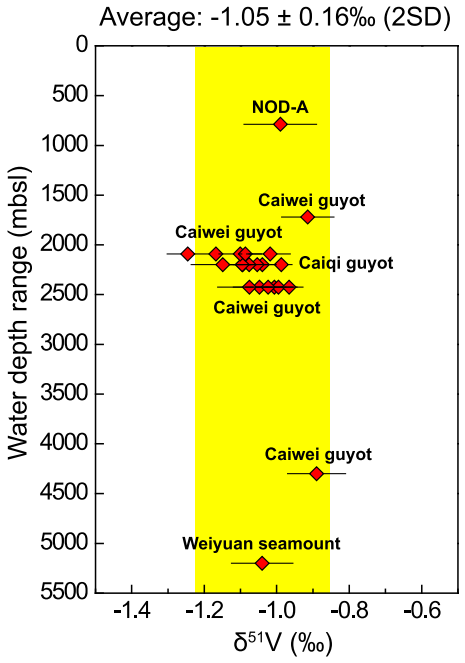

Fig. 5. Vanadium isotope variation in the non-phosphatized upper layers of Fe-Mn crusts and hydrogenetic Fe-Mn nodule NOD-A in relation to water depth. The yellow area shows estimated average $\delta^{51}V$ of near modern hydrogenetic Fe-Mn crusts and nodules and its error with two standard deviations (2 SD) of multiple measurements of the samples.

suggests that V isotope fractionation could occur among V species with different valance states and coordinated environment (Wu et al., 2015). In an oxic and a weakly alkaline (pH = 7–8) ocean, V is mainly present as V(V), which forms vanadate oxyanion in natural seawater (e.g. Peacock and Sherman, 2004). Vanadium isotope fractionation between vanadate oxyanion species (HVO_4^{2-} and $H_2VO_4^-$) may be negligible because they have the same coordinated environment (four-fold coordination numbers) and similar average V-O bond length (Wu et al., 2015). Conversely, the light V isotope (^{50}V) is preferentially adsorbed on the surface of iron oxyhydroxide (Wu et al., 2015), which is consistent with the observation that hydrogenetic Fe-Mn crusts and nodules have uniformly lower $\delta^{51}V$ than seawater. The preferent enrichment of ^{50}V in the Fe-Mn oxyhydroxide is potentially related to the lower V–O bond strength in the adsorption surface complexes compared to the vanadate in seawater (Wu et al., 2015). However, the observed offset in this dataset (-1.2 ± 0.2‰, 2 SD) is smaller than the calculated values ($\Delta^{51}V_{dissolved-sorbed} = -2.1 \pm 0.4$‰, 2 SD, Wu et al., 2015). The primary oxyhydroxides in the hydrogenetic Fe-Mn crusts are principally composed of phyllomanganate (birnessite and vernadite) with amorphous ferric oxyhydroxide (e.g., Glasby, 2006), while the theoretical values were calculated for fractionation between vanadate and the adsorption onto goethite. Thus, the difference between the observation and theoretical values might reflect a mineralogical control of V isotope fractionation during adsorption. Future experimental studies are required to better constrain the mineralogical fractionation.

The current model of the marine mass balance for V in ocean suggests that authigenic enrichment of V in oxic sediment accounts for about half of the total burial flux of V from modern oceans (Morford and Emerson, 1999). Dunlea et al (2015) also shows that pelagic sediments from sites across the South Pacific Gyre have higher V/Al than typical continental material. They further ascribe the enrichment of authigenic V in the pelagic sediments to the accumulation of V with Fe-Mn oxyhydroxide sediment components and/or oxyhydroxide coatings on pre-existing particles in the water column (Dunlea et al., 2015). In this case, V isotope composition of Fe-Mn oxyhydroxide components in pelagic sediment should also be lower than that of seawater by about -1.2 ± 0.2‰. Oxic removal via sorption could thus drive the V isotope composition of seawater heavy relative to the source flux. This conclusion further

proves previous model of oceanic V isotope mass balance which suggests that the deposition and burial of sediments under oxic conditions is an important mechanism for removing light ^{50}V from seawater (Wu et al., 2019).

5.3. Vanadium isotope variations in the diagenetic Fe-Mn nodules

Deep-sea diagenetic Fe-Mn nodules have uniformly lighter V isotope compositions than hydrogenetic Fe-Mn crusts (Table 2). Furthermore, the $\delta^{51}V$ of the deep-water diagenetic nodules display a negative correlation with Mn/Fe ($R^2 = 0.85$, Fig. 4). This relationship indicates that nodules with a strong diagenetic signature (e.g., high Mn/Fe) also have more negative $\delta^{51}V$. The shift of V isotope compositions with intensified diagenetic imprint could reflect: (1) phase transition of Fe-Mn oxyhydroxide by diagenetic alteration, which altered the mineralogy and V isotope composition of the original hydrogenetic minerals, or (2) isotope fractionation caused by the release of V along with Fe-Mn oxyhydroxide reduction and dissolution in sub-oxic porewaters and their transportation and deposition to form diagenetic Fe-Mn nodules.

It is well known that marine Fe-Mn crusts and nodules with different genesis show mineralogical diversity. Hydrogenic Fe-Mn crusts are mainly composed of phyllomanganate (birnessite and vernadite) and ferric oxyhydroxides, while diagenetic Fe-Mn nodules are mainly comprised of 10 Å manganates (buserite and todorokite) (e.g., Glasby, 2006). The principal Mn oxyhydroxide minerals in different types of Fe-Mn oxyhydroxide crusts and nodules have distinctive structure that control the surface adsorption behaviors and crystal-chemistry of various elements (e.g. Li, Ni; Jiang et al., 2007; Peacock, 2009). It is well known that isotope fractionation varies with mineralogy during mineral adsorption (e.g. Goldberg et al., 2009). Thus, V isotope variations of nodules might be the result of the structural diversity between main Mn oxyhydroxide phases of hydrogenetic crusts (birnessite and vernadite) and diagenetic nodules (10 Å manganates). However, the nodule sample NOD-A has a $\delta^{51}V$ value similar to hydrogenic Fe-Mn crust, although the high Li abundance (Fig. 3) may only be accommodated in the crystal structures of large tunnel-structures found in todorokite (Jiang et al., 2007). Thus, it is difficult to explain the V isotope composition of NOD-A if we regard the mineralogy of the Mn oxyhydroxide as the main control on the variation of V isotopes in diagenetic ferromanganese nodules. On the other hand, the concentrations of transition metals (Cu, Zn, and Ni) and the REE pattern both indicate that NOD-A is derived from seawater rather than pore fluids (Bau et al., 2014). In comparison, the correlation between transition metal contents (such as Cu, Ni, Zn and V) and Mn/Fe ratios in Fe-Mn crusts and nodules from Weiyuan seamount (Fig. 3) indicate the various contributions of pore fluids. Thus, the negative correlation between V isotope variations in Fe-Mn nodules and Mn/Fe ratios is more likely controlled by source contribution (seawater vs. pore fluids) during their formation rather than a mineralogical control.

Pore fluids are considered as the most important source of metals for diagenetic Fe-Mn nodules (e.g. Dymond et al., 1984). The variations of Tl isotope compositions in diagenetic nodules were explained by the adsorption of Tl from pore fluids in a closed-system reservoir of limited size (Rehkämper et al., 2002). To test whether this mechanism can also explain the observed V isotope variations in diagenetic nodules, we use a batch closed system model to test V isotope fractionation during adsorption. The model is similar to the Tl isotope model used in Rehkämper et al. (2002). Diagenetic Fe-Mn nodule growth mainly occurs in zones where the upward migration of reduced Mn^{2+} pore fluids are re-oxidized (Kuhn et al., 2017). Considering that the redox potential of V(V)-V(IV) couple is close to that of Fe(III)-Fe(II) and lower than that of Mn(IV)-Mn(II) in seawater (e.g. Bonatti et al., 1971; Piper and Calvert, 2009), it is highly unlikely the reduction of pentavalent V species and related isotope fractionation could largely occur in zones where there is Mn^{2+} transportation and deposition. We thus consider adsorption of V on the surface of Mn oxyhydroxides as the dominant process to control V isotope fractionation within pore fluid and thus the fractionation factor α is set at 0.9988 based on our inferred V isotope fractionation between hydrogenic Fe-Mn crusts and seawater. The partition coefficient of V between Fe-Mn oxyhydroxide and pore fluid ($D_{\text{Fe-Mn oxyhydroxide/fluid}}$) is set at 3.5×10^5 based on the estimation from the V contents in seawater and Fe-Mn crusts, which is close to the estimated distribution coefficients of V between manganese oxyhydroxides and seawater by a previous study (5.7×10^5, Takematsu et al., 1985). The main purpose of this model is to provide a first approximation to the concentration and isotope variations of V during closed-system adsorption. We set the initial concentration to seawater-like values of $c_{l,0} = 35$ nM (Jeandel et al., 1987; Ho et al., 2018), and tested the model varying different initial value of $\delta^{51}V_{l,0}$ between seawater (0.20‰) and hydrogenetic ferromanganese crusts and nodules (−1.05‰) endmember. Also, the growth and trace-metal composition of diagenetic-type precipitates is largely controlled by the diffusivity of pore fluids from underlying sediments (Calvert and Price, 1977; Dymond et al., 1984). Thus, it is reasonable to assume that the $\delta^{51}V$ of pore fluids are between the endmember values of seawater and hydrogenetic ferromanganese crusts and nodules. The assumed seawater composition may underestimate the V concentration of pore fluids given the remobilization of V with Mn and Fe recycling during early diagenesis, which will cause an increase of V concentration within pore fluids (Shaw et al., 1990; Morford et al., 2005). However, the direction of the trend lines of the modeling results will not change with the variations of initial composition and is not dependent on either of these assumptions. The results of these calculations are summarized and compared with the analytical data in Fig. 6. The model shows that the nodules with more diagenetic deposition from pore fluids (i.e. high Mn/Fe ratio and low V concentration) should have more positive $\delta^{51}V$ value. Such a trend contradicts our data (Fig. 6). Thus, it is unlikely that the V isotope variations in diagenetic nodules can be completely explained by varying the proportion of V adsorption in a closed-system reservoir.

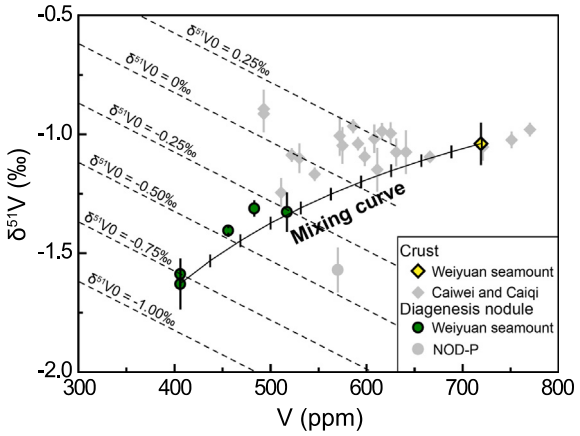

Fig. 6. Batch adsorption model for the V isotope variations of diagenetic Fe-Mn nodules by the adsorption of V in a closed-system reservoir. The initial concentration of porewater was set as seawater-like values of $c_{l,0} = 35$ nM, and various initial $\delta^{51}V$ value of pore water from seawater (0.20‰, Wu et al., 2019) to the hydrogenetic Fe-Mn crusts and nodules (−1.05‰) endmember was set to run the model (shown with dotted lines). Model results are shown with dotted lines. Solid line shows binary mixing trends between hydrogenetic Fe-Mn crust (V = 719 ppm, $\delta^{51}V = -1.04$‰) and diagenesis Fe-Mn nodule endmember (V = 406, $\delta^{51}V = -1.63$‰) from C-C zone. Increment of mixing curves (vertical bar) is 10%. Results for additional Fe-Mn crust and nodule samples are also shown for comparison.

Instead, the range of $\delta^{51}V$ of the Fe-Mn crusts and nodules from Weiyuan seamount can be most easily explained by a mixing of hydrogenetic and diagenetic endmembers. Therein, the V content (719 ppm) and $\delta^{51}V$ (−1.04‰) of the crust samples from C-C zone are used as the hydrogenetic endmember, representing water column supplied V, and the V content (406 ppm) and $\delta^{51}V$ (−1.63‰) of the nodules from C-C zone with the highest Mn/Fe ratio are used as the diagenetic endmember, representing sediment pore water supplied V. Mixing between such endmembers does reproduce the observed variations in $\delta^{51}V$ (Fig. 6). Such mixing processes may be appropriate for deep-sea nodules, since the diagenetic metals are likely supplied episodically during the stirring of bottom sediments along with the continuous supply of hydrogenous metal ions to form the Fe-Mn nodules (Jung and Lee, 1999). The diagenetic endmember $\delta^{51}V$ value might reflect the isotopic fractionation that occurred during diffuse/transportation of V in the pore water and its scavenging by diagenetic Fe-Mn oxyhydroxide afterwards. Further studies of pore water analyses providing sedimentary profiles are necessary to better understand V isotope fractionation during early diagenesis.

5.4. Depth profile of V isotope variations in Fe-Mn crusts

The depth profile of crusts from Caiwei guyot (such as Dive70B OJ113-211T) displays a negative V isotope shift in the deeper and thus older portions of the Fe-Mn crusts (Fig. 7). It is noteworthy that the older portions of the Fe-Mn crusts are imprinted by phosphatization with high Ca and P contents, with the replacement of carbonate in Fe-Mn crust pore space by carbonate fluorapatite (CFA) (e.g. Hein et al., 1993). The CFA imprint on the primary crust material could modify the bulk composition of the crust. Previous leaching experiment showed that the CFA phase in Fe-Mn crust contains negligible V (Koschinsky and Hein, 2003). Thus, the primary V isotope composition in the Fe-Mn crust might not be modified during phosphatization, if such a process only results from the admixture of CFA to the primary crust material. Some studies also suggest that phosphatization of Fe-Mn crusts occurred under less-oxidizing conditions (Koschinsky and Halbach, 1995; Nishi et al., 2017). Previous study shows that the phosphatized layers display more abundant Ni, Cu, and Zn, higher Mn/Fe ratio and lower Co concentrations relative to non-phosphatized layers in the Fe-Mn crust profile (Nishi et al., 2017). Such geochemical features are suggested to indicate that phosphatized layers formed under less-oxidizing conditions due to diagenetic influence (Nishi et al., 2017). Thus, it is possible that the post-depositional phosphatization altered the original V isotope compositions. However, not all the studied phosphatized layers in the curst profiles show isotope deviation and the layer with the highest phosphorus content (6.42 wt.%) has a $\delta^{51}V$

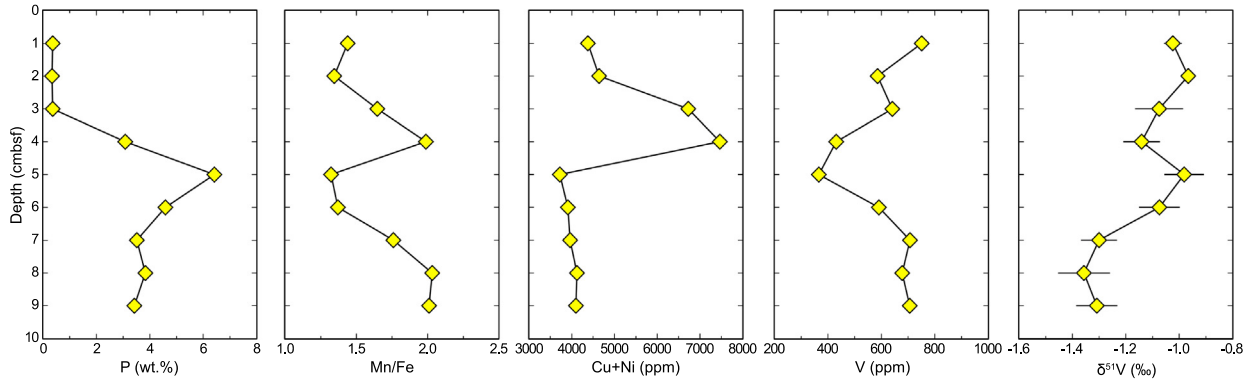

Fig. 7. Depth profile of selected elements and V isotope composition in the Fe-Mn crust Dive70B OJ113-211T from Caiwei guyot (West Pacific). A marked positive shift in V isotope ratios is observed, which is in irrelevant to the variations of P, Cu + Ni, V contents.

value (-0.98 ± 0.07‰) indistinguishable from the overlying younger layers (-1.08‰ to -0.97‰; Fig. 7). In addition, the phosphatized layers with lighter δ^{51}V values do not document an enrichment of Ni, Cu or Zn, although they have higher Mn/Fe ratios (1.76–2.03) than all the layers except one (1.32–1.65) with "modern" δ^{51}V values (Fig. 7 and Table 2). Thus, it seems unlikely that V isotope variations of the Fe-Mn crust profile could be simply explained as the results of diagenetic deposition along with phosphatization. Partial reduction and dissolution of the Fe-Mn oxyhydroxide phases might also occur under less-oxidizing condition, which could result in the diagenetic remobilization and reorganization of elements within the Fe-Mn crusts (Koschinsky et al., 1997). Although no obvious evidence of such diagenetic modification is found in our samples, we cannot definitively rule out its potential influence on the V isotope documents in the phosphatized layers, which needs further study.

It is also possible that the V isotope variations observed in the sample Dive70B OJ113-211T are primary. If this is the case, the V isotope shift in the Fe-Mn crust profile might reflect the variation of the isotope fractionation factor between seawater and Fe-Mn crust over time with an invariant seawater isotope composition. The isotope fractionation factor might vary due to external parameters such as temperature, salinity or pH. Because Fe-Mn oxyhydroxides only form under oxic conditions, the dominant V species was likely vanadate when the phosphatized layers formed. Thus, the variations of isotope fractionation cannot be explained by the change of V species in seawater. The temperature change in the deep ocean would be minimal and thus also unlikely to change the isotope fractionation. In addition, it is difficult to ascribe the isotope variations to only mineralogical controls, as previously discussed. Thus, it is most likely that the V isotope variations in the depth profile of Fe-Mn crust are not caused by the changes in isotope fractionation factor.

Alternatively, the observed V isotope variations of the Fe-Mn crust profile might reflect the evolving seawater V isotope compositions. These temporal changes could record a global signal due to the relatively long residence time of V with respect to the ocean mixing time (Morford and Emerson, 1999). Because the size of the sedimentary V sink is predicted to vary with the redox state of the depositional environments (Wu et al., 2015), it is expected that the isotopic mass-balance for vanadium in the ocean is controlled by the global redox state of the ocean (Wu et al., 2019). Recent investigations showed that the low-maturity crude oil samples with high V/(Ni + V) ratio and high S, which were thought to be sourced in highly anoxic sediments (Lewan, 1984), have δ^{51}V values of about -0.4 to 0‰ (Gao et al., 2018), more positive than that of Fe-Mn crust. This observation provides some clues that V removal under reducing conditions might have an isotope composition closer to seawater e.g. less fractionated. Thus, the observed negative V isotope shift of the Fe-Mn crust data, could be reflecting an increase in the area of permanently seafloor thus increasing the burial of V in reducing sediments. It is noteworthy that the phosphatization on mid-Pacific seamounts occurred during the time periods between 36 and 12 Ma and with a peak event occurred at the Eocene/Oligocene transition (~34 Ma) (Hein et al., 1993; Hyeong et al., 2013), which is thought to be linked with the expansion of the oxygen-minimum zone (OMZ) and suboxic conditions (Halbach, 1989; Koschinsky et al., 1997). Thus, the light V isotope composition in the Fe-Mn crusts depth profile might be related to this phosphatization event and reflect the change of in global circulation of oxygenated bottom waters at that time (Halbach, 1989; Nishi et al., 2017). This is a speculative interpretation as we do not have well constrained age information for these samples. In addition, a well constrained marine V isotope mass balance is required to better interpret the paleoceanography implications for the observed V isotope shift. Furthermore, we cannot definitively rule out the influence of diagenesis during phosphatization on the primary V isotope signature of Fe-Mn crust (as discussed before). Future measurement and comparison of multiple individual Fe-Mn crust profiles with well-constrained age information will be helpful to test these hypotheses. Experimental studies are also necessary to confirm V isotope fractionation during adsorption of V with Fe and Mn oxyhydroxide. Despite these uncertainties, our results show the great potential to apply hydrogenous Fe-Mn crusts as archives to record V isotope variations of seawater provided fractionations remain consistent. Importantly, this study provides an important foundation to build the marine V isotope mass balance as Fe-Mn oxyhydroxides are the dominate V sink in the modern oxic ocean.

6. SUMMARY

We conducted the first systematic V isotope analyses of Fe-Mn crusts and nodules exhibiting large V isotope variations from which we conclude the following:

(1) The younger non-phosphatized layers of hydrogenetic Fe-Mn crust and hydrogenous Fe-Mn nodules have limited V isotope variations with average value of -1.05 ± 0.16‰ (2 SD), regardless of sampling location and water depth. Such results imply a relatively homogeneous V isotope composition of marine hydrogenetic Fe-Mn crusts and nodules.
(2) The hydrogenetic Fe-Mn crusts and nodules are depleted in ^{51}V compared with seawater. This offset is potentially the result of isotope fractionation during the adsorption of V onto Fe-Mn particles with fractionation factor of -1.2 ± 0.2‰ (2 SD). Thus, burial of V with Fe-Mn oxyhydroxides precipitation is an important isotopically light sink in the modern ocean.
(3) Fe-Mn nodules have large V isotope variations with δ^{51}V values ranging between -0.98‰ to -1.65‰. This variability can be explained by the variable contribution of V from diagenetic and hydrogenetic precipitation. Because these diagenetic nodules are affected by the chemistry within the underlying sediment, they may not record the primary seawater V isotope signature.

(4) Vanadium isotope variations are observed in the depth profile of a Fe-Mn crusts. Although we cannot definitevely rule out the possibility that diagenetic remobilization and reorganization in the phosphatized layers modify the primary V isotope signature. However, if the observed $\delta^{51}V$ depth profiles record V isotope seawater variations, this is likely controlled by the redox-related seawater V mass balance. Thus, our results imply that the $\delta^{51}V$ records of hydrogenous Fe-Mn crusts can provide insights into ancient ocean chemistry.

ACKNOWLEDGMENT

We thank Weixin Lv for help in the laboratory. We would like to acknowledge support from the National Basic Research Program of China (973 Program) [2015CB755905], National Natural Science Foundation of China [41630206], Science Fund for Creative Research Groups of the National Natural Science Foundation of China [41721002], the Natural Science Foundation of Zhejiang Province of China (No. LQY18D060002), the Scientific Research Fund of the Second Institute of Oceanography, MNR (NO. JG1803). JDO acknowledges support from National Science Foundation grant OCE 1434785. We are thankful to the first scientific Cruise of manned submersible of China 'Jiao Long'. This manuscript has benefited from reviews by Ann Dunlea, two anonymous reviewers and editorial handling of Silke Severmann.

APPENDIX A. SUPPLEMENTARY MATERIAL

Supplementary data to this article can be found online at https://doi.org/10.1016/j.gca.2019.09.007.

REFERENCES

Algeo T. J. (2004) Can marine anoxic events draw down the trace element inventory of seawater? *Geology* **32**, 1057–1060.

Algeo T. J. and Maynard J. B. (2004) Trace-element behavior and redox facies in core shales of Upper Pennsylvanian Kansas-type cyclothems. *Chem. Geol.* **206**, 289–318.

Atkins A. L., Shaw S. and Peacock C. L. (2014) Nucleation and growth of todorokite from birnessite: Implications for trace-metal cycling in marine sediments. *Geochim. Cosmochim. Acta* **144**, 109–125.

Barling J. and Anbar A. D. (2004) Molybdenum isotope fractionation during adsorption by manganese oxides. *Earth Planet. Sci. Lett.* **217**, 315–329.

Bau M., Schmidt K., Koschinsky A., Hein J., Kuhn T. and Usui A. (2014) Discriminating between different genetic types of marine ferro-manganese crusts and nodules based on rare earth elements and yttrium. *Chem. Geol.* **381**, 1–9.

Bischoff J. L., Heath G. R. and Leinen M. (1979) *Geochemistry of Deep-sea Sediments from the Pacific Manganese Nodule Province: DOMES Sites A, B, and C, Marine Geology and Oceanography of the Pacific Manganese Nodule Province*. Springer, pp. 397–436.

Bonatti E., Fisher D., Joensuu O. and Rydell H. (1971) Postdepositional mobility of some transition elements, phosphorus, uranium and thorium in deep sea sediments. *Geochim. Cosmochim. Acta* **35**, 189–201.

Bonatti E. (1972) Classification and genesis of submarine iron-manganese deposits. *Ferromanganese deposits on the ocean floor*, 149–166.

Breit G. N. and Wanty R. B. (1991) Vanadium accumulation in carbonaceous rocks – a review of geochemical controls during deposition and diagenesis. *Chem. Geol.* **91**, 83–97.

Calvert S. and Price N. (1977) Geochemical variation in ferromanganese nodules and associated sediments from the Pacific Ocean. *Mar. Chem.* **5**, 43–74.

Collier R. W. (1984) Particulate and dissolved vanadium in the North Pacific Ocean. *Nature* **309**, 441–444.

Dunlea A. G., Murray R. W., Sauvage J., Spivack A. J., Harris R. N. and D'Hondt S. (2015) Dust, volcanic ash, and the evolution of the South Pacific Gyre through the Cenozoic. *Paleoceanogr. Paleoclimatol.* **30**, 1078–1099.

Dymond J., Lyle M., Finney B., Piper D. Z., Murphy K., Conard R. and Pisias N. (1984) Ferromanganese nodules from MANOP Sites H, S, and R—Control of mineralogical and chemical composition by multiple accretionary processes. *Geochim. Cosmochim. Acta* **48**, 931–949.

Elderfield H. and Schultz A. (1996) Mid-ocean ridge hydrothermal fluxes and the chemical composition of the ocean. *Annu. Rev. Earth Pl. Sc.* **24**, 191–224.

Emerson S. R. and Huested S. S. (1991) Ocean anoxia and the concentrations of molybdenum and vanadium in seawater. *Mar. Chem.* **34**, 177–196.

Flanagan, F.J., Gottfried, D., 1980. USGS rock standards; III, Manganese-nodule reference samples USGS-Nod-A-1 and USGS-Nod-P-1 (No. 1155). US Govt. Print Off.

Frank M., O'nions R., Hein J. and Banakar V. (1999) 60 Myr records of major elements and Pb–Nd isotopes from hydrogenous ferromanganese crusts: reconstruction of seawater paleochemistry. *Geochim. Cosmochim. Acta* **63**, 1689–1708.

Gall L., Williams H., Siebert C., Halliday A., Herrington R. and Hein J. (2013) Nickel isotopic compositions of ferromanganese crusts and the constancy of deep ocean inputs and continental weathering effects over the Cenozoic. *Earth Planet. Sci. Lett.* **375**, 148–155.

Gao Y., Casey J. F., Bernardo L. M., Yang W. and Bissada K. A. (2018) Vanadium isotope composition of crude oil: effects of source, maturation and biodegradation. *Geol. Soc., London, Spec. Publ.* **468**, 83–103.

Glasby G. (2006) Manganese: Predominant role of nodules and crusts. In *Marine Geochemistry* (eds. H. Schulz and M. Zabel). Springer, Berlin Heidelberg, pp. 371–427.

Goldberg T., Archer C., Vance D. and Poulton S. W. (2009) Mo isotope fractionation during adsorption to Fe (oxyhydr)oxides. *Geochim. Cosmochim. Acta* **73**, 6502–6516.

Gueguen B., Rouxel O., Rouget M.-L., Bollinger C., Ponzevera E., Germain Y. and Fouquet Y. (2016) Comparative geochemistry of four ferromanganese crusts from the Pacific Ocean and significance for the use of Ni isotopes as paleoceanographic tracers. *Geochim. Cosmochim. Acta* **189**, 214–235.

Halbach P., Hebisch U. and Scherhag C. (1981) Geochemical variations of ferromanganese nodules and crusts from different provinces of the Pacific Ocean and their genetic control. *Chem. Geol.* **34**, 3–17.

Halbach P. (1989) Co-rich and platinum bearing manganese crust deposits on seamounts: nature, formation and metal potential. *Mar. Min.* **8**, 23–39.

Hein J. R., Yeh H. W., Gunn S. H., Sliter W. V., Benninger L. M. and Wang C. H. (1993) Two major Cenozoic episodes of phosphogenesis recorded in equatorial Pacific seamount deposits. *Paleoceanography* **8**, 293–311.

Hein J. R., Koschinsky A., Halbach P., Manheim F. T., Bau M., Kang J.-K. and Lubick N. (1997) Iron and manganese oxide

mineralization in the Pacific. *Geol. Soc., London, Spec. Publ.* **119**, 123–138.

Hein J. R., Koschinsky A., Bau M., Manheim F. T., Kang J.-K. and Roberts L. (2000) Cobalt-rich ferromanganese crusts in the Pacific. *Handbook Mar. Miner. Deposits* **18**, 239–273.

Hein, J.R., Koschinsky, A., 2014. Deep-ocean ferromanganese crusts and nodules, pp. 273–291.

Heller C., Kuhn T., Versteegh G. J., Wegorzewski A. V. and Kasten S. (2018) The geochemical behavior of metals during early diagenetic alteration of buried manganese nodules. *Deep Sea Res. Part I* **142**, 16–33.

Ho P., Lee J.-M., Heller M. I., Lam P. J. and Shiller A. M. (2018) The distribution of dissolved and particulate Mo and V along the US GEOTRACES East Pacific Zonal Transect (GP16): The roles of oxides and biogenic particles in their distributions in the oxygen deficient zone and the hydrothermal plume. *Mar. Chem.* **201**, 242–255.

Horner Tristan J., Williams Helen M., Hein James R., Saito Mak A., Burton Kevin W., Halliday Alex N. and Nielsen Sune G. (2015) Persistence of deeply sourced iron in the Pacific Ocean. *Proc. Natl. Acad. Sci. U.S.A.* **112**(5), 1292–1297. https://doi.org/10.1073/pnas.1420188112.

Huang J.-H., Huang F., Evans L. and Glasauer S. (2015) Vanadium: Global (bio)geochemistry. *Chem. Geol.* **417**, 68–89.

Hyeong K., Kim J., Yoo C. M., Moon J.-W. and Seo I. (2013) Cenozoic history of phosphogenesis recorded in the ferromanganese crusts of central and western Pacific seamounts: Implications for deepwater circulation and phosphorus budgets. *Palaeogeogr. Palaeoclimatol. Palaeoecol.* **392**, 293–301.

Jeandel C., Caisso M. and Minster J. F. (1987) Vanadium behaviour in the global ocean and in the Mediterranean sea. *Mar. Chem.* **21**, 51–74.

Jiang X., Lin X., Yao D., Zhai S. and Guo W. (2007) Geochemistry of lithium in marine ferromanganese oxide deposits. *Deep Sea Res. Part I* **54**, 85–98.

Jung H.-S. and Lee C.-B. (1999) Growth of diagenetic ferromanganese nodules in an oxic deep-sea sedimentary environment, northeast equatorial Pacific. *Mar. Geol.* **157**, 127–144.

Koschinsky A. and Halbach P. (1995) Sequential leaching of marine ferromanganese precipitates: Genetic implications. *Geochim. Cosmochim. Acta* **59**, 5113–5132.

Koschinsky A., Stascheit A., Bau M. and Halbach P. (1997) Effects of phosphatization on the geochemical and mineralogical composition of marine ferromanganese crusts. *Geochim. Cosmochim. Acta* **61**, 4079–4094.

Koschinsky A. and Hein J. R. (2003) Uptake of elements from seawater by ferromanganese crusts: solid-phase associations and seawater speciation. *Mar. Geol.* **198**, 331–351.

Kuhn T., Wegorzewski A., Rühlemann C. and Vink A. (2017) Composition, formation, and occurrence of polymetallic nodules. *Deep-Sea Mining. Springer*, 23–63.

Lewan M. D. and Maynard J. B. (1982) Factors controlling enrichment of vanadium and nickel in the bitumen of organic sedimentary rocks. *Geochim. Cosmochim. Acta* **46**, 2547–2560.

Ling H., Burton K., O'nions R., Kamber B., Von Blanckenburg F., Gibb A. and Hein J. (1997) Evolution of Nd and Pb isotopes in Central Pacific seawater from ferromanganese crusts. *Earth Planet. Sci. Lett.* **146**, 1–12.

Menendez A., James R. H., Lichtschlag A., Connelly D. and Peel K. (2019) Controls on the chemical composition of ferromanganese nodules in the Clarion-Clipperton Fracture Zone, eastern equatorial Pacific. *Mar. Geol.* **409**, 1–14.

Morford J. L. and Emerson S. (1999) The geochemistry of redox sensitive trace metals in sediments. *Geochim. Cosmochim. Acta* **63**, 1735–1750.

Morford J., Emerson S., Breckel E. and Kim S. (2005) Diagenesis of oxyanions (V, U, Re, and Mo) in pore waters and sediments from a continental margin. *Geochim. Cosmochim. Acta* **69**, 5021–5032.

Nielsen S. G., Mar-Gerrison S., Gannoun A., LaRowe D., Klemm V., Halliday A. N., Burton K. W. and Hein J. R. (2009) Thallium isotope evidence for a permanent increase in marine organic carbon export in the early Eocene. *Earth Planet. Sci. Lett.* **278**, 297–307.

Nielsen S. G., Prytulak J. and Halliday A. N. (2011) Determination of precise and accurate 51V/50V isotope ratios by MC-ICP-MS, part 1: chemical separation of vanadium and mass spectrometric protocols. *Geostand. Geoanal. Res.* **35**, 293–306.

Nielsen S. G., Prytulak J., Wood B. J. and Halliday A. N. (2014) Vanadium isotopic difference between the silicate Earth and meteorites. *Earth Planet. Sci. Lett.* **389**, 167–175.

Nielsen S. G., Owens J. D. and Horner T. J. (2016) Analysis of high-precision vanadium isotope ratios by medium resolution MC-ICP-MS. *J. Anal. At. Spectrom.* **31**, 531–536.

Nielsen S. G., Auro M., Righter K., Davis D., Prytulak J., Wu F. and Owens J. D. (2019) Nucleosynthetic vanadium isotope heterogeneity of the early solar system recorded in chondritic meteorites. *Earth Planet. Sci. Lett.* **505**, 131–140.

Nishi K., Usui A., Nakasato Y. and Yasuda H. (2017) Formation age of the dual structure and environmental change recorded in hydrogenetic ferromanganese crusts from Northwest and Central Pacific seamounts. *Ore Geol. Rev.* **87**, 62–70.

Peacock C. L. and Sherman D. M. (2004) Vanadium(V) adsorption onto goethite (α-FeOOH) at pH 1.5 to 12: a surface complexation model based on ab initio molecular geometries and EXAFS spectroscopy. *Geochim. Cosmochim. Acta* **68**, 1723–1733.

Peacock C. L. (2009) Physiochemical controls on the crystal-chemistry of Ni in birnessite: Genetic implications for ferromanganese precipitates. *Geochim. Cosmochim. Acta* **73** (12), 3568–3578.

Piper D. and Calvert S. (2009) A marine biogeochemical perspective on black shale deposition. *Earth Sci. Rev.* **95**, 63–96.

Prytulak J., Nielsen S. G. and Halliday A. N. (2011) Determination of precise and accurate 51V/50V isotope ratios by multi-collector ICP-MS, Part 2: Isotopic composition of six reference materials plus the allende chondrite and verification tests. *Geostand. Geoanal. Res.* **35**, 307–318.

Prytulak J., Nielsen S. G., Ionov D. A., Halliday A. N., Harvey J., Kelley K. A., Niu Y. L., Peate D. W., Shimizu K. and Sims K. W. W. (2013) The stable vanadium isotope composition of the mantle and mafic lavas. *Earth Planet. Sci. Lett.* **365**, 177–189.

Prytulak J., Sossi P. A., Halliday A. N., Plank T., Savage P. S. and Woodhead J. D. (2017) Stable vanadium isotopes as a redox proxy in magmatic systems? *Geochem. Perspect. Lett.* **3**, 75–84.

Qi Y. H., Wu F., Ionov D. A., Puchtel I. S., Carlson R. W., Nicklas R. W., Yu H. M., Kang J. T., Li C. H. and Huang F. (2019) Vanadium isotope composition of the Bulk Silicate Earth: constraints from peridotites and komatiites. *Geochim. Cosmochim. Acta* **259**, 288–301.

Rehkämper M., Frank M., Hein J. R., Porcelli D., Halliday A., Ingri J. and Liebetrau V. (2002) Thallium isotope variations in seawater and hydrogenetic, diagenetic, and hydrothermal ferromanganese deposits. *Earth Planet. Sci. Lett.* **197**, 65–81.

Rehkämper M. and Nielsen S. G. (2004) The mass balance of dissolved thallium in the oceans. *Mar. Chem.* **85**, 125–139.

Rudnick R. L. and Gao S. (2003) Composition of the continental crust. In The Crust, Treatise in Geochemistry (ed. R. L. Rudnick). vol. 3, pp. 1–64.

Schuth S., Horn I., Brüske A., Wolff P. E. and Weyer S. (2017) First vanadium isotope analyses of V-rich minerals by femtosecond laser ablation and solution-nebulization MC-ICP-MS. *Ore Geol. Rev.* **81**, 1271–1286.

Schuth S., Brüske A., Hohl S. V., Jiang S. Y., Meinhardt A. K., Gregory D. D., Viehmann S. and Weyer S. (2019) Vanadium and its isotope composition of river water and seawater: Analytical improvement and implications for vanadium isotope fractionation. *Chemical Geology*.

Shaw T. J., Gieskes J. M. and Jahnke R. A. (1990) Early diagenesis in differing depositional environments: The response of transition metals in pore water. *Geochim. Cosmochim. Acta* **54**, 1233–1246.

Shiller A. M. and Boyle E. A. (1987) Dissolved vanadium in rivers and estuaries. *Earth Planet. Sci. Lett.* **86**, 214–224.

Takematsu N., Sato Y., Okabe S. and Nakayama E. (1985) The partition of vanadium and molybdenum between manganese oxides and sea water. *Geochim. Cosmochim. Acta* **49**, 2395–2399.

Ventura G. T., Gall L., Siebert C., Prytulak J., Szatmari P., Hürlimann M. and Halliday A. N. (2015) The stable isotope composition of vanadium, nickel, and molybdenum in crude oils. *Appl. Geochem.* **59**, 104–117.

Wanty R. B. and Goldhaber M. B. (1992) Thermodynamics and kinetics of reactions involving vanadium in natural systems: Accumulation of vanadium in sedimentary rocks. *Geochim. Cosmochim. Acta* **56**, 1471–1483.

Wegorzewski A. V. and Kuhn T. (2014) The influence of suboxic diagenesis on the formation of manganese nodules in the Clarion Clipperton nodule belt of the Pacific Ocean. *Mar. Geol.* **357**, 123–138.

Wehrli B. and Stumm W. (1989) Vanadyl in natural waters: Adsorption and hydrolysis promote oxygenation. *Geochim. Cosmochim. Acta* **53**, 69–77.

Wu F., Qin T., Li X., Liu Y., Huang J.-H., Wu Z. and Huang F. (2015) First-principles investigation of vanadium isotope fractionation in solution and during adsorption. *Earth Planet. Sci. Lett.* **426**, 216–224.

Wu F., Qi Y., Yu H., Tian S., Hou Z. and Huang F. (2016) Vanadium isotope measurement by MC-ICP-MS. *Chem. Geol.* **421**, 17–25.

Wu F., Qi Y., Perfit M. R., Gao Y., Langmuir C. H., Wanless V. D., Yu H. and Huang F. (2018) Vanadium isotope compositions of mid-ocean ridge lavas and altered oceanic crust. *Earth Planet. Sci. Lett.* **493**, 128–139.

Wu F., Owens J. D., Huang T., Sarafian A., Huang K.-F., Sen I. S., Horner T. J., Blusztajn J., Morton P. and Nielsen S. G. (2019) Vanadium isotope composition of seawater. *Geochim. Cosmochim. Acta* **244**, 403–415.

Xue Y., Li C.-H., Qi Y., Zhang C., Miao B. and Huang F. (2018) The vanadium isotopic composition of L ordinary chondrites. *Acta Geochim.* **37**, 501–508.

Associate editor: Silke Severmann